JOURNAL OF PROPULSION AND POWER
Vol. 12, No. 3, May–June 1996

# Upwind Unstructured Scheme for Three-Dimensional Combusting Flows

Ashvin Hosangadi,* Robert A. Lee,* Brian J. York,* Neeraj Sinha,† and Sanford M. Dash‡
*Combustion Research and Flow Technology, Inc., Dublin, Pennsylvania 18917*

**As an interim step towards the development of a hybrid upwind structured/unstructured solver for combusting/multiphase flowfields, the TRI3D unstructured code of Barth has been extended to analyze multicomponent combusting flows. The extensions mimic the Roe/total variation diminishing (TVD) based thermochemical extensions in the structured solver, CRAFT, and entail a strong coupling of chemical species equations and complete linearization of the chemical source term, treated in a fully implicit manner. Issues regarding the quality of solutions obtained using locally one-dimensional Riemann flux procedures and TVD limiters are more pronounced in unstructured formulations and are dealt with in depth in this article. Comparative studies of structured and unstructured analyses of laminar premixed flames, ducted shock-induced combustion, and blunt-body shock-induced combustion serve to delineate these issues and the need for solution adaptive gridding and improved flux limiters to capture flame zones properly.**

## Introduction

OVER the past several years, the development of structured Navier–Stokes codes has matured to the point that they now include advanced thermochemical and multiphase capabilities within an upwind/implicit framework. In contrast, unstructured codes have generally been explicit and applied to ideal-gas flowfields, with much of the developmental work focusing on the unstructured aspects of data structure and connectivity algorithms. The application of unstructured codes to propulsive/combustion flowfields entails the inclusion of real-gas thermophysics and chemical kinetics. The compatibility of both numerics and thermophysics between structured and unstructured codes is critical in providing a framework for the development of hybrid structured/unstructured (S/U) schemes for propulsive applications. Hybrid schemes are optimal for complex problems involving multibody interactions and/or transient dynamic flows, since they combine the advantages of structured implicit numerics about each body and unstructured explicit numerics in the intervening free shear regions, permitting the use of adaptive embedding techniques. An unstructured solver with an upwind flux procedure for generalized multispecies systems would provide a stepping-stone towards the development of a hybrid solver, addressing the issue of numerical compatibility at the structured/unstructured interface where discontinuities and waves cross S/U domains. The need for a generalized unstructured solver for a variety of applications has been the impetus for the research described in this article, which emphasizes the complex problem area of shock-induced combustion.

The extension of unstructured algorithms to real-gas flows is an area of current interest and is being pursued independently by several researchers.[1-3] Applebaum et al.[1] present a flux-split[4] upwind methodology for real-gas flows, which allows for nonequilibrium between the vibrational and the translational/rotational energies. However, the time-integration procedure updates primitive nonconservative variables rather than the conservative variables. While this is computationally less intensive, since it eliminates the need for an iterative temperature decoding procedure, nonconservative dependent variables are not ideal for high Mach number flows with strong shocks. Weiss and Murthy[2] employ a preconditioned equation system that preserves a well-conditioned system from low Mach numbers to mildly supersonic flows. The flux computation procedure employed is not an upwind formulation, and flux limiting is not enforced on the higher-order gradients; both of these factors make it more sensitive to artificial viscosity issues at higher Mach numbers. Yu et al.[3] present a finite element based scheme for extremely low-speed flows where a constant pressure condition is assumed, and the species and energy diffusion equations are solved. The primary drawback of the finite volume schemes discussed previously (Refs. 1 and 2), as a vehicle for further development, is that their data and flux computation structure are cell-face-based. While a face-based scheme is the natural choice for two-dimensional calculations, it becomes impractical for three-dimensional cases. As discussed next, an edge-based scheme provides a more efficient framework for three-dimensional geometries and was chosen as the basis for our scheme.

The unstructured framework adapted for our scheme is an edge-based cell-vertex data structure with a finite volume dual defined for each vertex. For three-dimensional cases, the edge-based data structure is significantly superior to a cell-centered, face-based data structure.[5-8] In an edge-based scheme, the number of vertices is smaller than the number of cells, and the number of edges are lower than the number of faces, thereby reducing both the memory requirements as well as the flux computations significantly.[5] In the research described, the edge-based data structure has been taken from Barth,[5] who has formulated efficient vectorized and parallelized edge-based operations for viscous[9] and inviscid fluxes, and has also incorporated a preconditioned sparse implicit solver for ideal-gas flows. The work described utilizes only the explicit run option. The focus of this study is on the numerical and physical issues entailed in incorporating generalized thermochemistry within this edge-based formulation; an in-depth study of the numerical accuracy of unstructured solvers for shock-induced combusting flows is described. For all of the cases presented in

Presented as Paper 95-0258 at the AIAA 33rd Aerospace Sciences Meeting and Exhibit, Reno, NV, Jan. 10–13, 1995; received March 17, 1995; revision received Oct. 23, 1995; accepted for publication Nov. 27, 1995. 

*Senior Research Scientist, 174 North Main Street, Building 3, P.O. Box 1150. Member AIAA.

†Vice President and Director of Technology, 174 North Main Street, Building 3, P.O. Box 1150. Member AIAA.

‡President and Chief Scientist, 174 North Main Street, Building 3, P.O. Box 1150. Member AIAA.

this article, the fidelity of the unstructured solution is compared with that obtained from the structured code, CRAFT, which has similar numerics.[10,11] This critical evaluation of the two reacting solutions for similar grid resolution permits us to assess the relative accuracy of the two procedures and highlights the need for dynamic grid adaption in unstructured solvers on a routine basis.

In the following sections, a brief overview of the edge-based cell-vertex data structure for three-dimensional tetrahedral cells is provided, followed by a description of the governing equations, chemical kinetics procedure, and flux-differencing for this system where the fluid, species, and other scalar equations (e.g., turbulence transport) are solved in a strongly coupled conservative form. Subsequently, an in-depth discussion of numerical dissipation and total variation diminishing-(TVD-) limiting issues within the unstructured framework is provided. The accuracy of captured flame zones in high-speed flows is found to be sensitive to the specifics of the flux limiter employed, and modifications to the baseline limiter for reacting flow cases are presented that provided marked improvements. The modified flux formulation is employed to compute representative shock-induced combustion cases. For these calculations, we compare both with experimental data (where available), and, with solutions obtained using the structured code, CRAFT, with similar grid resolution. We conclude by discussing future work with multiphase formulations and hybrid S/U interfacing, steps toward developing a comprehensive tool for propulsion/combustion applications.

### Edge-Based Unstructured Framework

In this section, we give a brief overview of the edge-based connectivity logic derived from Barth's unstructured code TRI3D,[5,9,12] and refer the reader to his works for additional details. The flow variables are defined at the vertices of each unstructured cell (Fig. 1); in this article we have restricted our attention to tetrahedral cells while the framework permits generalized unstructured cells. The scheme is based on a finite volume procedure wherein an appropriate dual or control volume is defined around each vertex (see Fig. 1). Barth[5] defines the control volume as a polyhedron obtained from the union of all tetrahedra that are incident to the given vertex. This definition allows all operations to be based on edge-based information that may then be adapted for either vector or parallel machines for efficient computing (see Ref. 10 for details). The flux is computed at each dual face using the higher-order estimates of the dependent variables at each dual face.

The higher-order estimate of the dependent variables at the dual face is obtained by computing their gradient at the cell vertices and using this value to extrapolate the variables to the dual face. A number of different options have been developed to evaluate the flow gradients including the Green–Gauss procedure,[5,13] linear reconstruction, and other higher-order gradient procedures.[1,5,8] For the work described, we have employed a linear reconstruction gradient calculation procedure as proposed by Barth.[5] The gradient is computed assuming that the flow-dependent variables $Q$ are varying linearly within the dual and provides second-order accuracy at the interface. To suppress spurious oscillations, the gradient is limited to yield a TVD scheme. The implementation of the TVD procedure is most critical for reacting flows because of its impact on the smearing of the contact surfaces and the flame front. This issue is discussed in detail in a later section.

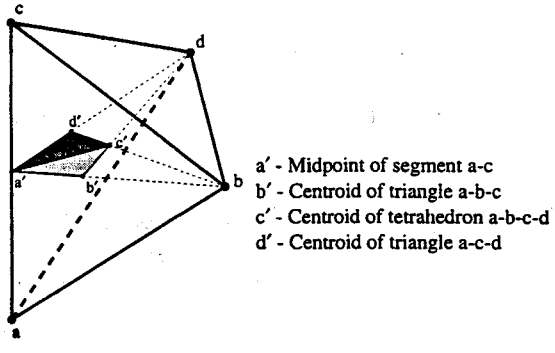


**Fig. 1 Contribution to vector area $s_{ac}$ from tetrahedron a–b–c–d.**

### Governing Equations

The integral form of the conservation equations over each vertex dual $\Omega$ is given as follows:

$$\frac{\mathrm{d}(QV)_i}{\mathrm{d}t} + \int_{\partial\Omega_i} \boldsymbol{F}(\boldsymbol{Q}, \boldsymbol{n})\,\mathrm{d}s = \int_{\Omega_i} \boldsymbol{D}\,\mathrm{d}v \tag{1}$$

Following standard notation, $\boldsymbol{Q}$ is the vector of dependent variables, $\boldsymbol{F}(\boldsymbol{Q}, \boldsymbol{n})$ is the flux vector expression for a given $Q$ and local dual vector area $\boldsymbol{n}$, and $\boldsymbol{D}$ is the chemical kinetic source term. Attention is focused on the inviscid flux vectors in this article while noting that the viscous fluxes have been formulated within the edge-based formulation.[9] The vectors $\boldsymbol{Q}$, $\boldsymbol{F}$, and $\boldsymbol{D}$ are defined as

$$\boldsymbol{Q} = \begin{bmatrix} \rho \\ \rho u \\ \rho v \\ \rho w \\ e \\ \rho_1 \\ \vdots \\ \rho_s \\ \vdots \\ \rho_{\mathrm{NS}-1} \end{bmatrix}, \quad \boldsymbol{F}(\boldsymbol{Q}, \boldsymbol{n}) = \begin{bmatrix} \rho U \\ (\rho U u + n_x P) \\ (\rho U v + n_y P) \\ (\rho U w + n_z P) \\ (e + P)U \\ \rho_1 U \\ \vdots \\ \rho_s U \\ \vdots \\ \rho_{\mathrm{NS}-1} \end{bmatrix} \tag{2}$$

$$\boldsymbol{D} = \begin{bmatrix} 0 \\ 0 \\ 0 \\ 0 \\ 0 \\ \dot{\omega}_1 \\ \vdots \\ \dot{\omega}_s \\ \vdots \\ \dot{\omega}_{\mathrm{NS}-1} \end{bmatrix}$$

Here, the first five equations are the conservation of mixture mass $\rho$, the three components of momentum, and total internal energy per unit volume $e$, $\{e = \rho[h + 0.5(u^2 + v^2 + w^2)] - P\}$. The subsequent equations solve for the partial densities $\rho_s$ for (NS − 1) chemical species out of a total of NS species that are solved. The partial density of the NSth species $\rho_{\mathrm{NS}}$, is determined by the mass balance for the mixture density:

$$\left(\sum_{s=1}^{\mathrm{NS}-1} \rho_s + \rho_{\mathrm{NS}} = \rho\right)$$

In the flux vector $\boldsymbol{F}(\boldsymbol{Q}, \boldsymbol{n})$, the volumetric flux through each dual face $U$ is defined as $(U = n_x u + n_y v + n_z w)$, where $n_x$, $n_y$, and $n_z$ are the components of the vector dual area in the $x$, $y$, and $z$ direction, respectively. In the source term $D$, $\dot{\omega}_s$ is the chemical production term.

The equation of state for the gaseous mixture follows Dalton's law of partial pressure given as follows:

$$P = \frac{\rho \bar{R} T}{M}, \qquad \left[M = \left(\sum_{s=1}^{\mathrm{NS}} \frac{c_s}{M_s}\right)^{-1}\right] \tag{3}$$

Here, $c_s$ is the mass fraction of the $i$th species ($c_s = \rho_s/\rho$). The enthalpy of the mixture is obtained from the following summation of the individual enthalpies:

$$h = \sum_{s=1}^{NS} c_s[h_s^{of} + h_s(T)], \qquad \left[h_s(T) = \int_0^T C_{P_s}(T)\, dT\right] \tag{4}$$

Note that the species enthalpy includes the heat of formation $h_s^{of}$ in addition to the sensible enthalpy $h_s(T)$, and implicitly defines the heat release when reactions occur. The specific heat $[C_{P_s}(T)]$ of each species is allowed to vary as a function of temperature. The enthalpy and specific heats are specified in tabular form using the JANNAF thermochemical data bank. The tabular values are then fitted with a cubic spline to obtain a generalized functional relationship. To decode the temperature from the internal energy at each new time step, an iterative Newton–Raphson procedure is employed.

The chemical source term is specified by restricting our attention to conventional laminar chemistry, given by the law of mass action for each reaction,

$$\dot{\omega}_s = M_s \sum (\nu'' - \nu') \left(K_f \prod \alpha^{\nu'} - K_b \prod \alpha^{\nu''}\right) \tag{5}$$

where ($\alpha_s = \rho_s/M_s$) is the molar concentration of species $s$, and $\nu'$, $\nu''$ are the stoichiometric coefficients for each chemical reaction. The forward and backward are specified in Arrhenius form as

$$K(T) = \exp(\ell n\, C_1 + C_2/T + C_3\, \ell n\, T) \tag{6}$$

where reaction rates $C_1$, $C_2$, and $C_3$ are selected from generalized reaction data banks. For the reacting cases presented in this article, we selected a hydrogen–air chemistry set from the data bank. The specific set employed is a reduced mechanism described by Evans and Schnexnayder,[14] which models seven species and eight reactions (see Table 1).

**Upwind Flux Computation**

The first step in the evaluation of the flux is to obtain higher-order estimates of the flow variables at the dual face. To obtain this estimate, the gradient reconstruction is performed on the following nonconservative variable set:

$$\tilde{Q} = (\rho, u, v, w, T, c_1, \ldots, c_s, \ldots, c_{NS-1})^T \quad (c_s = \rho_s/\rho) \tag{7}$$

Note that the primitive variable temperature is chosen because the enthalpy at the dual face is obtained as a simple summation of individual species enthalpies. The more appealing choice, from a physical viewpoint, is to work with the total enthalpy since the total enthalpy varies linearly across strong velocity gradients (making the linear reconstruction exact), while the temperature does not. However, this would be prohibitively expensive since the temperature would have to be decoded iteratively at each dual face. Having computed the gradient $\tilde{Q}$, the reconstructed values at the dual face are obtained as

$$\begin{aligned} Q_m^- &= Q_0 + (\nabla\tilde{Q})_{v_0} \cdot (r_m - r_0) \\ Q_m^+ &= Q_0 + (\nabla\tilde{Q})_{v_i} \cdot (r_m - r_i) \end{aligned} \tag{8}$$

Here, $r_m = 0.5 \times (r_0 + r_i)$ is the median of the edge $e_{0i}$ associated with the dual face. Both $Q_m^-$ and $Q_m^+$ are the discontinuous estimates of the flow variables on either side of the dual face, which now readily lends itself to a Riemann problem.

The Riemann problem at the dual face is computed with a Roe-averaged, flux-differenced solver,[15] which defines the flux $F_m$ as

$$\begin{aligned} F_m = \tfrac{1}{2}[&F(Q_m^-, \boldsymbol{n}_{0i}) + F(Q_m^+, \boldsymbol{n}_{0i}) + \Delta F^-(Q_{Roe}^m, \boldsymbol{n}_{0i}) \\ &+ \Delta F^+(Q_{Roe}^m, \boldsymbol{n}_{0i})] \end{aligned} \tag{9}$$

where $\boldsymbol{n}_{0i}$ is the vector area of the dual face crossing edge $e_{0i}$, and the subscript Roe denotes Roe-averaged variables. The flux differences $\Delta F^-$ and $\Delta F^+$ are given as

$$\Delta F^+(Q_{Roe}^m, \boldsymbol{n}_{0i}) = \tfrac{1}{2}[R_{Roe}^m(\Lambda + |\Lambda|)_{Roe} L_{Roe}^m](Q_m^+ - Q_m^-) \tag{10}$$

$$\Delta F^-(Q_{Roe}^m, \boldsymbol{n}_{0i}) = \tfrac{1}{2}[R_{Roe}^m(\Lambda - |\Lambda|)_{Roe} L_{Roe}^m](Q_m^+ - Q_m^-) \tag{11}$$

Here, $R$ and $L$ are, respectively, the right and left eigenvector matrices, while $\Lambda$ is the diagonal eigenvalue matrix. The flux differences defined in Eqs. (10) and (11) require well-posed eigenvalues. To prevent the eigenvalues from going to zero, the entropy fix is invoked by defining the absolute eigenvalues to be

$$|\lambda| = \sqrt{\lambda^2 + \varepsilon^2} \tag{12}$$

where $\varepsilon$ is a small number typically set to 0.1. The Roe-averaged variables required to compute the flux differences are not defined for real-gas mixtures, with the original derivation by Roe[15] being valid for a single-component ideal-gas.

In our study, an approximate quadrature formula is employed following the analysis of Liu and Vinokur.[16] Liu and Vinokur have derived an approximate procedure to satisfy Roe criteria for real-gas mixtures that yields the correct acoustic speed at the interface and retains the shock-capturing features. This derivation was first implemented by Molvik[17] in his three-dimensional structured code, TUFF, which formed the basis for CRAFT,[10,11] the structured code used in this study for validation and comparison purposes. For a real-gas mixture, the velocities, total enthalpy, and species mass fractions continue to be averaged in the classical Roe format as

$$y_{Roe} = \frac{y^+\sqrt{\rho^+} + y^-\sqrt{\rho^-}}{\sqrt{\rho^+} + \sqrt{\rho^-}}$$
$$[y \in (u, v, w, H, c_1, \ldots, c_s, \ldots, c_{NS-1})] \tag{13}$$

(Note that in the previous equation, and for the subsequent discussion here, the subscript $m$ is dropped for simplicity of notation.) In addition to these variables, additional Roe-averaged thermodynamic variables required at the interface (for defining $R_{Roe}$, $L_{Roe}$, and $\Lambda_{Roe}$) are $\gamma$, acoustic speed $a$, and a variable $D_s$, defined as follows:

$$D_s = (\gamma - 1)h_s - (\gamma RT/M_s), \qquad (s = 1, NS) \tag{14}$$

These Roe-averaged quantities are obtained by first making an initial guess, and then projecting these approximate values onto a hyperplane in state space such that they satisfy the Roe

**Table 1 Hydrogen–air rates, $k = AT^n \exp(-\Theta/T)$**

| Reactions | Evans and Schnexnayder[14] | | |
|---|---|---|---|
| | $A$ | $n$ | $\Theta$ |
| 1. $OH + H_2 \rightarrow H + H_2O$ | $2.0 \times 10^{13}$ | 0 | 2600 |
| 2. $H + O_2 \rightarrow O + OH$ | $2.19 \times 10^{14}$ | 0 | 8455 |
| 3. $O + H_2 \rightarrow H + OH$ | $7.5 \times 10^{13}$ | 0 | 5586 |
| 4. $H + OH + M \rightarrow H_2O + M$ | $4.39 \times 10^{20}$ | −1.5 | 0 |
| 5. $H + H + M \rightarrow H_2 + M$ | $1.799 \times 10^{18}$ | −1.0 | 0 |
| 6. $H + O + M \rightarrow OH + M$ | $7.1 \times 10^{18}$ | −1.0 | 0 |
| 7. $O + O + M \rightarrow O_2 + M$ | $4.0 \times 10^{17}$ | −1.0 | 0 |
| 8. $OH + OH \rightarrow O + H_2O$ | $5.3 \times 10^{12}$ | 0 | 503 |

criteria. The initialized values for these variables are given as the following simple arithmetic averages:

$$\hat{a} = (a^+ + a^-)/2, \quad \hat{\gamma} = (\gamma^+ + \gamma^-)/2, \quad \hat{D}_s = (D_s^+ + D_s^-)/2 \tag{15}$$

Using these initial estimates, the Roe-averaged value of these thermodynamic variables is obtained as

$$D_{s,\text{Roe}} = \frac{\hat{D}_s - \hat{a}^4 \Delta\rho_s \delta P/\chi}{1 - \Delta P \delta P/\chi} \qquad (s = 1, \text{NS}) \tag{16}$$

$$\gamma_{\text{Roe}} = \frac{\hat{\gamma} - 1}{1 - \Delta p \delta P/\chi} + 1 \tag{17}$$

where the $\Delta$ operator is defined as $\Delta(y) = y^+ - y^-$. The operators $\delta P$ and $\chi$ are given as follows:

$$\delta P = \Delta P + \sum_{s=1}^{\text{NS}} \hat{D}_s \Delta\rho_i - (\hat{\gamma} - 1)[\Delta(\rho h) - \Delta P] \tag{18}$$

$$\chi = \sum_{s=1}^{\text{NS}} (\hat{a}^2 \Delta\rho_s)^2 + (\Delta P)^2 \tag{19}$$

The Roe-averaged $\gamma_{\text{Roe}}$ and $D_{s,\text{Roe}}$ values finally yield the acoustic speed of the mixture at the dual interface as

$$a_{\text{Roe}} = \sqrt{(\gamma_{\text{Roe}} - 1)h_{\text{Roe}} - \sum_{s=1}^{\text{NS}} c_{s,\text{Roe}} D_{s,\text{Roe}}} \tag{20}$$

The computational efficiency of the upwind procedure outlined previously depends primarily on our ability to vectorize the matrix multiplications ($L\Lambda R$) within the constraints of the edge-based formulation. Vectorization is particularly important for the strongly coupled formulation employed here, where the block size of the matrices increases as $[5 + (\text{NS} - 1)] \times [5 + (\text{NS} - 1)]$, where NS is the number of species being modeled. The edge-based formulation sorts the edges into bins such that no two edges in a bin come to a common vertex point. Having colored the edges in this fashion, the flux operations are carried out for all edges with the same color. Hence, to vectorize operations within each colored bin, the matrix multiplication loops would have to be unwound by the compiler. On the Cray C-90, the maximum loop size unwound is 5, preventing the real-gas formulation from vectorizing. To overcome this problem, $R$, $L$, and $\Lambda$ were subdivided into smaller matrices where the block size of each matrix is no greater than 5 (see schematic in Fig. 2). The net product was obtained as the sum of the submatrix products that now unwind and allow the outer edge loop to vectorize. The speed up obtained with this procedure was a factor of 5, with the code operating at an average of 270 Mflops for the real-gas formulation.

The time-integration of Eq. (1) is performed with an explicit four-step Runge–Kutta procedure. The chemical source term is treated implicitly to overcome source-term stiffness for fast reactions. The complete source-term Jacobian is evaluated including its dependence on mixture temperature and individual species concentrations. For the supersonic cases presented in this article, freestream conditions were imposed at the inflow specifying all of the flow conditions. At the supersonic outflow boundaries, all flow properties are extrapolated from within the flow domain. At solid walls, standard reflection conditions are imposed to ensure zero normal convective flux. For other applications involving subsonic inflow and outflow, we have incorporated characteristic-based, nonreflective boundary conditions that allow waves to cross the boundaries without generating oscillations.[11]

## TVD Limiting and Numerical Accuracy Issues

In this section, we discuss numerical accuracy and dissipation issues that arise with unstructured algorithms. The quality of solutions obtained using upwind unstructured algorithms is adversely affected by the following two numerical issues: 1) the locally one-dimensional Riemann flux procedure at the dual faces and 2) TVD-limiting technique for higher-order schemes. Both of these issues are of major concern in structured grid solvers as well. However, these problems are exacerbated in unstructured algorithms where the grids are inherently skewed with respect to the wave/shock propagation fronts. We elaborate on both of these issues in our discussion and present techniques on alleviating their impact.

The first issue with the flux computation arises because the upwind procedure in this code (and other upwind codes in general) is based on a locally one-dimensional Riemann problem, which assumes that the shock is propagating normal to the face at which the flux is being computed. If this assumption is incorrect and the face is skewed relative to the propagation direction, we introduce an error because we are applying normal shock relations rather than the correct oblique shock relations. In a structured grid, for relatively simple flow geometries, we attempt to align the grid with the approximate propagation direction, thereby reducing the error in the flux at the faces. However, this is not possible in an unstructured tetrahedral grid where grid faces are inherently skewed relative to the wave propagation direction. Consider, for example, a simple one-dimensional shock-tube problem. A structured solver employing a quadrilateral element will have zero net flux even if a strong shock passes through the element because the normal vector

$$\boldsymbol{n} = \begin{bmatrix} 1 & 0 & 0 \\ 0 & 1 & 0 \\ 0 & 0 & 1 \end{bmatrix}$$

zeros out the fluxes in the other directions.

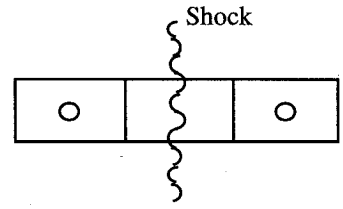


However, for an unstructured tetrahedral element, when a shock passes through the element, the sum of the Roe-averaged net flux at the dual edges does not necessarily zero-out, and numerical error occurs.

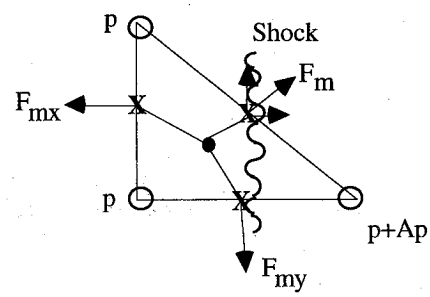


This numerical error increases the smearing around the shock front and also deteriorates its convergence to steady state. To alleviate this problem within the current flux procedure, the unstructured grid would routinely have to be adapted around

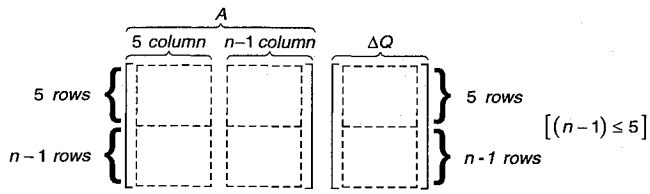


**Fig. 2 Schematic diagram of matrix subdivision process illustrated for vectorized matrix multiplication $A\Delta Q$.**

strong gradients to reduce the amplitude of the spurious velocity spikes. A longer-term solution entails utilizing a more physically correct multidimensional upwinding procedure, which is an area of current research interest.[18]

The numerical dissipation and convergence characteristics of the scheme are also affected by the specifics of the TVD limiter employed. In particular, for reacting-flow cases, the TVD procedure is a critical factor in computing the flame front location. This was particularly true for high-speed, shock-induced combustion cases, where TVD procedures originally proposed for ideal-gas cases generated smaller flame induction zones because of the smearing of the contact surface, even though the shock itself was captured fairly accurately. The TVD procedure had to be modified to reduce the smearing of the scalar species equations and obtain the correct flame separation from the shock.

The TVD limiter is designed to enforce a monotonic behavior by enforcing the restriction that the reconstructed value not exceed the maximum and minimum of neighboring nodal values. For instance, consider a variable $u$ whose gradient is computed as $\nabla u_0$ at node 0. Let $u_i$ be the reconstructed value of $u$ at a dual face; it is defined as

$$u_i = u_0 + (\nabla u)\cdot(r_i - r_0) \tag{21}$$

To obtain a monotonic scheme, the gradient $\nabla u$ is multiplied by a limiting value $\phi_0$ (Ref. 5), such that

$$\Phi_0 = \begin{cases} \min\left(1, \dfrac{u_0^{\max} - u_0}{u_i - u_0 + \varepsilon}\right), & \text{if } u_i - u_0 > 0 \\ \min\left(1, \dfrac{u_0^{\min} - u_0}{u_i - u_0 + \varepsilon}\right), & \text{if } u_i - u_0 < 0 \\ 1 & \text{if } u_i - u_0 = 0 \end{cases} \tag{22}$$

where $\varepsilon$ is a small number to prevent spurious limiting in regions of constant value.

The drawback of the limiter given in Eq. (22) is that it limits the gradient $\nabla u$ even in regions of smooth, but sharp, gradients, such as is the case for the radical species mass fraction in the flame induction zone. As a result, in regions of sharp, but continuous, gradients, the scheme reduces to first-order accuracy. To illustrate this, consider supersonic inflow into a duct with a bump of 8.5 deg. Figure 3a shows the shock train resulting for an inflow Mach number of 3. Figure 3b shows the contours of the limiting factor $\phi$ in the duct for this flow. The minimum value of $\phi$ in this contour plot is approximately 0.35. More importantly, the limiting is clearly not confined to the shock regions, but extends into the regions with smooth flow gradients as well. The limiting factor in the smooth regions was approximately 0.7, and therefore, reduces the order of accuracy of the solution. To rectify the problem of the limiter triggering in smooth regions of the flow, Eq. (22) was modified as follows:

$$\Phi_0 = \begin{cases} \min\left(1, \dfrac{u_0^{\max} - u_0 + K\Delta r}{u_i - u_0 + \varepsilon}\right), & \text{if } u_i - u_0 > 0 \\ \min\left(1, \dfrac{u_0^{\min} - u_0 - K\Delta r}{u_i - u_0 + \varepsilon}\right), & \text{if } u_i - u_0 < 0 \\ 1 & \text{if } u_i - u_0 = 0 \end{cases} \tag{23}$$

In Eq. (23) we have essentially prevented the limiter from triggering as long as the gradients are of the order of 1 (and $u_i - u_0 \cong 0(\Delta r)$, $\Delta r$ being a characteristic length for the dual under consideration), even if this implies that the difference exceeds the criteria set by $u_0^{\max}$ and $u_0^{\min}$. An arbitrary constant $K$ is set by the user to relax this condition; for the runs reported in this article, $K$ was set at 0.1. To illustrate the less stringent, but still monotonic, behavior of the modified limiter, we replot the limiting factor $\phi$ in Fig. 3c. It is readily apparent that the limiter is triggering locally in regions of the shock and is not limiting the value in the regions of the smooth gradients. Furthermore, the minimum limiter value even in the shock region is only 0.7, compared to about 0.35 for the original limiter. The pressure along the walls, as shown in Fig. 3d, clearly shows that the overall accuracy of the solution is enhanced with the modified limiter; the peak pressure values at the shocks with the original limiter are significantly lower than either the CRAFT solution or the solution with the new limiter.

The modified limiter presented here proved to be essential for reacting flow calculations. In high-speed shock-induced reacting flows, there is a sharp flame induction zone behind the shock where the free radicals grow exponentially. The flame induction zone is extremely sensitive to the numerical dissipation; if the free radical species mass fractions are smeared, the flame tends to burn too fast and not separate enough from the shock front. This was observed to be the case with the original limiter that was being triggered in the induction zone.

To illustrate the effect of the limiter on the flame capturing, we computed a one-dimensional laminar flame for a premixed hydrogen–air mixture with an inflow Mach number of 4 and a temperature of 1300 K. Figure 4 shows the grid-converged solution for the unstructured grid (dashed line) with the original limiter, and the solid line shows the grid-converged solution obtained using CRAFT, with the same limiter. For this simple case, the unstructured flame burns too fast and an examination of $\phi$ indicates that the limiter is indeed kicking in. The solution with the modified limiter is overlaid on Fig. 4 (dashed–dot line) and we now get nearly identical results for the structured and unstructured code. Furthermore, an inspection of the limiter values indicates that the $\phi$ values are 1, which indicates that the limiter is not being triggered after the steady-state solution has been achieved. The limiter does not influence the quality of the structured solution that has optimal grid alignment.

As a final observation, we note that neither of the limiter formulations [Eqs. (22) or (23)] is differentiable. The limiting values $\phi$ discontinuously trigger around shocks, thereby affecting convergence while eliminating oscillations even for strong shocks. A number of researchers have implemented modified forms of the van Albada limiter,[19] which is continuously differentiable. However, while this limiter improves convergence significantly, it does not preserve a monotonic solution around shocks. Clearly, the formulation of more efficient limiters at high speeds is an area of continuing research.

## Validation—Nonreacting Case

Transonic flow over a sphere–cylinder geometry is computed using the real-gas formulation for air (the mass fraction of $N_2$ is 0.767 and the mass fraction of $O_2$ is 0.232). The freestream Mach number of the gas is 0.95. The unstructured grid was generated with 1581 nodes on each axisymmetric plane with the grid extending 10 radii into the freestream. The pressure distribution on the body is compared with experimental data (taken from Ref. 20) in Fig. 5. The pressure at the stagnation point and along the sphere face matches the experimental value well. The expansion zone along the cylinder is slightly underpredicted by the unstructured solution, but is consistent with other Euler-structured code predictions reported in the literature.[20]

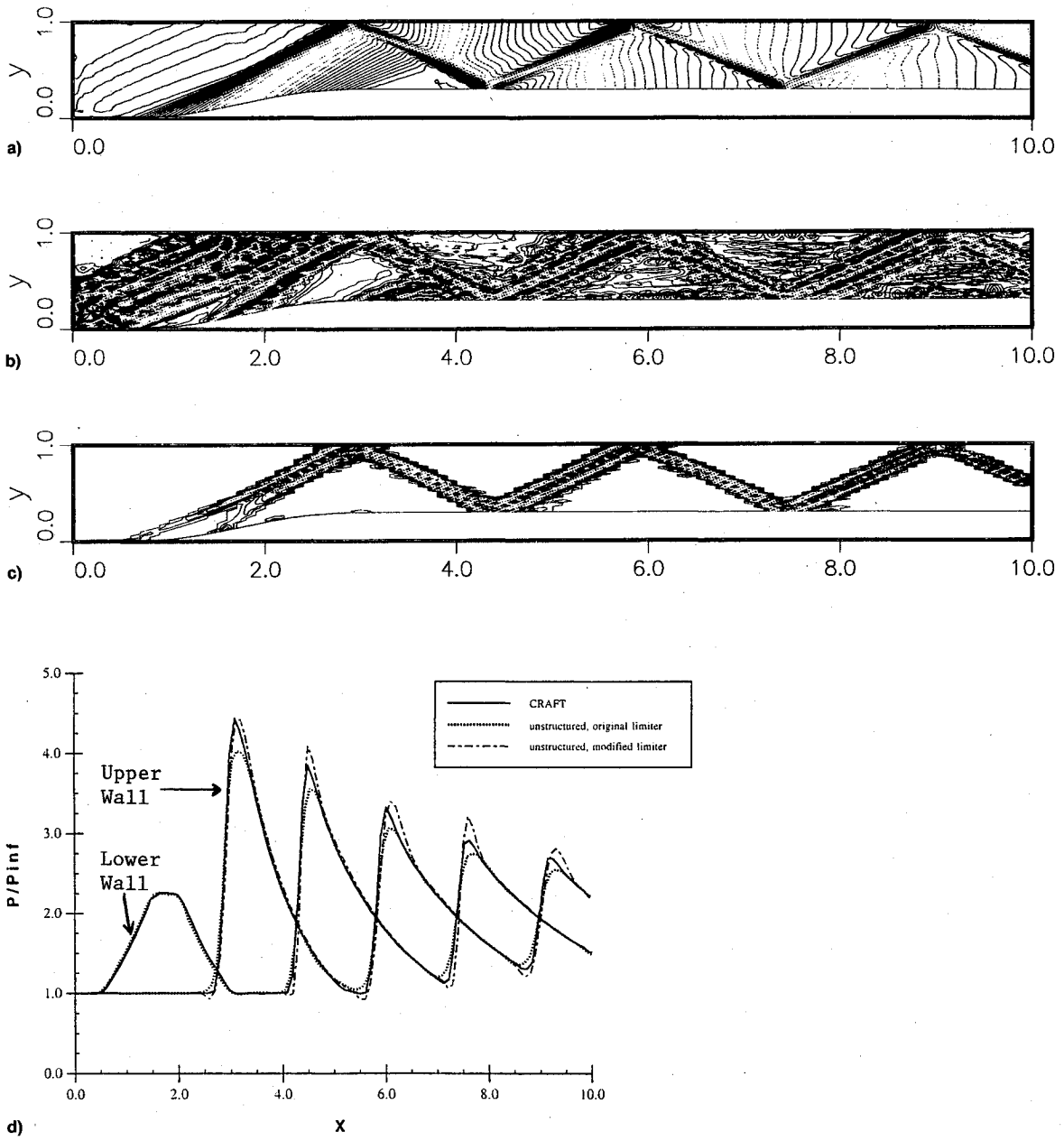


**Fig. 3 Comparison of unstructured prediction with experimental surface pressure data: a) pressure contours, b) original limiter contours, c) modified limiter contours, and d) shock train inside two-dimensional duct.**

## Shock-Induced Combustion Calculations

In this section, we present calculations for shock-induced combustion in premixed hydrogen–air flowfields. For both of these cases, we have used the seven-species/eight-reaction mechanism described in Ref. 17. The first test case is for a supersonic inflow over a sphere–cylinder geometry for which there is experimental data to validate the combustion results against. The second calculation is for supersonic inflow into a duct with a bump where the resulting shock train ignites the mixture. We note that although both flowfields are essentially two dimensional, they were run as three-dimensional calculations. In these calculations we focus on the numerical accuracy of the unstructured solver and for both calculations, we have compared the unstructured code results with a corresponding solution using our structured code, CRAFT, with similar grid resolution.

### Sphere-Cylinder Case

Shock-induced combustion in a stoichiometric mixture of hydrogen–air moving at Mach 6.46 into a sphere–cylinder geometry is computed. The diameter of the sphere is 15 mm. This computation simulates experiments performed by Lehr,[21] where visualization data is available to validate the numerical results. The premixed gas is at a pressure of 0.42 atm and a freestream temperature of 292 K. We note that this case, which has also been simulated by other investigators, is a rigorous test of the numerical accuracy of the thermochemical formulation; the location of the shock and flame front downstream (along the cylinder) is extremely sensitive to how well the induction zone is captured upstream on the spherical nose where the flame front is very close to the shock. Therefore, this test case gives us an opportunity to evaluate the effectiveness of the modified TVD limiter in regions of a sharp induction zone where the original limiter was inadequate. To conduct a careful assessment of the accuracy of the unstructured solver for specified grid resolutions, we have also used the solutions obtained from the structured code CRAFT as a benchmark. To make back-to-back comparisons, the unstructured code was run using two azimuthal planes of the structured grid, wherein each hexagonal cell was broken into six

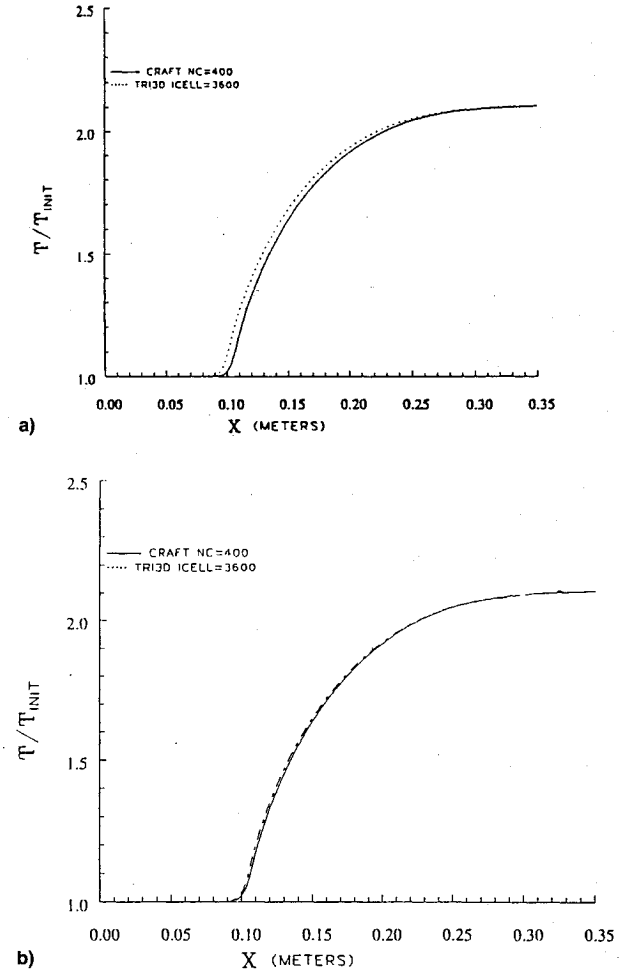


**Fig. 4 Laminar flame in one-dimensional premixed $H_2$–air flow: a) original and b) modified limiters.**

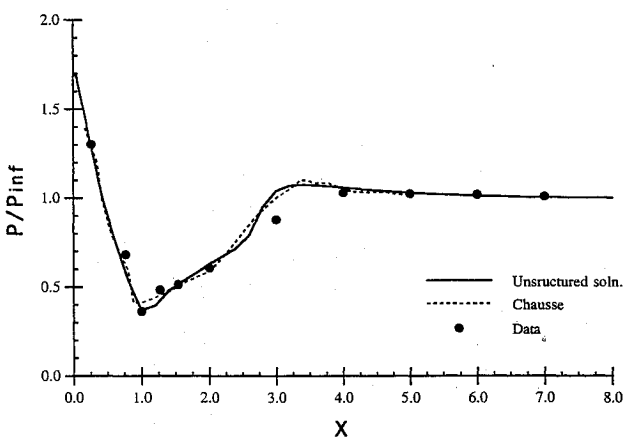


**Fig. 5 Transonic missile, surface pressure comparison.**

tetrahedral cells by drawing additional diagonal planes within the cell.

To obtain the baseline-structured solution and grid resolution for comparison, we computed this problem using CRAFT on an adapted 71 × 71 grid, shown in Fig. 6a, which is clustered in the region between the shock and the flame front. For this adapted grid, excellent comparison is obtained with the experimental data (Fig. 6b). The flame front separates from the shock downstream, indicating that the induction zone is captured adequately in the normal shock upstream. We note that the adapted grid was critical to obtain the correct solution for the structured code as described in Ref. 10.

The unstructured code was first run on the equivalent unstructured grid (5041 nodes on an azimuthal plane) using the identical nodal positions. Figure 7a shows the corresponding solution. Clearly, the flame front does not separate out adequately from the shock. Consequently, the shock does not turn as strongly either, and is located further away from the cylindrical surface of the body. This indicates that for similar grid resolutions, the unstructured solver is more dissipative than the corresponding structured solver with otherwise similar flux calculation procedures.

To evaluate grid-resolution sensitivity, the unstructured code was run by doubling the number of radial nodes, i.e., each azimuthal plane has 10,011 nodes corresponding to a 71 × 140 structured grid. The solution obtained with this finer grid is shown in Fig. 7b. Excellent agreement is now obtained with the experimental data. This would seem to indicate that the unstructured code needs almost twice as much resolution as an equivalent structured solver to capture the flame induction zone. The fact that the solution improved with grid resolution also indicates that the increased dissipation in the unstructured solver is coming from the inherent skewness of the unstructured grids while the modified TVD limiter is functioning ad-

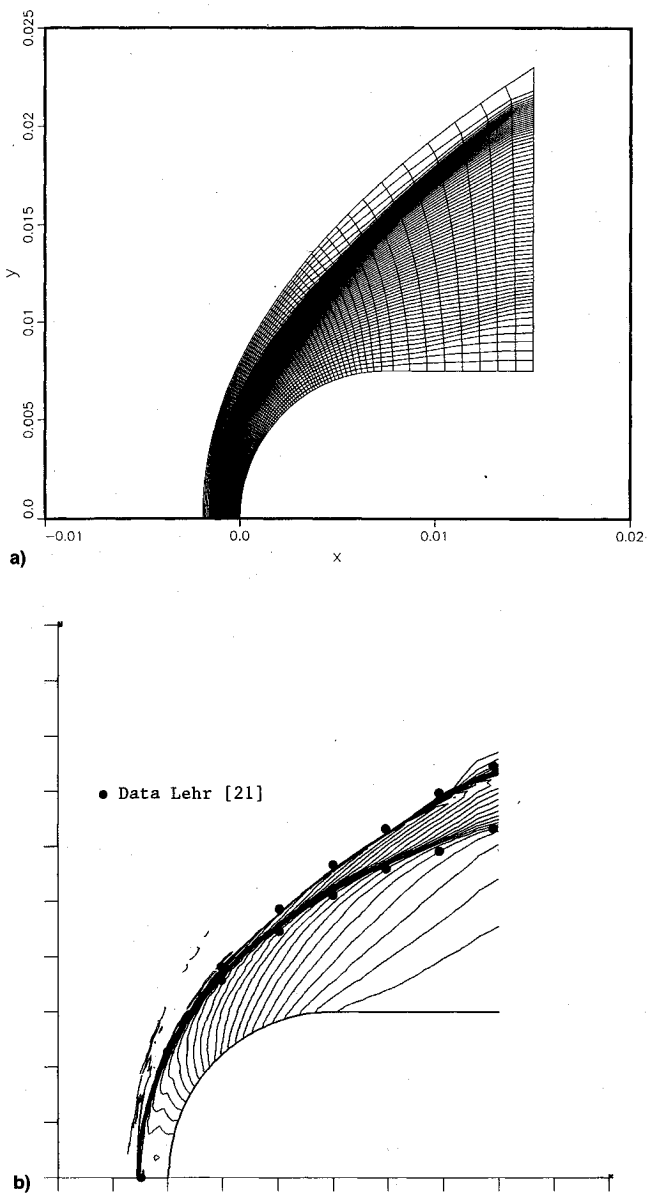


**Fig. 6 CRAFT simulation of blunt-body shock-induced combustion: a) structured adaptive grid and b) comparison of density contours with data.**

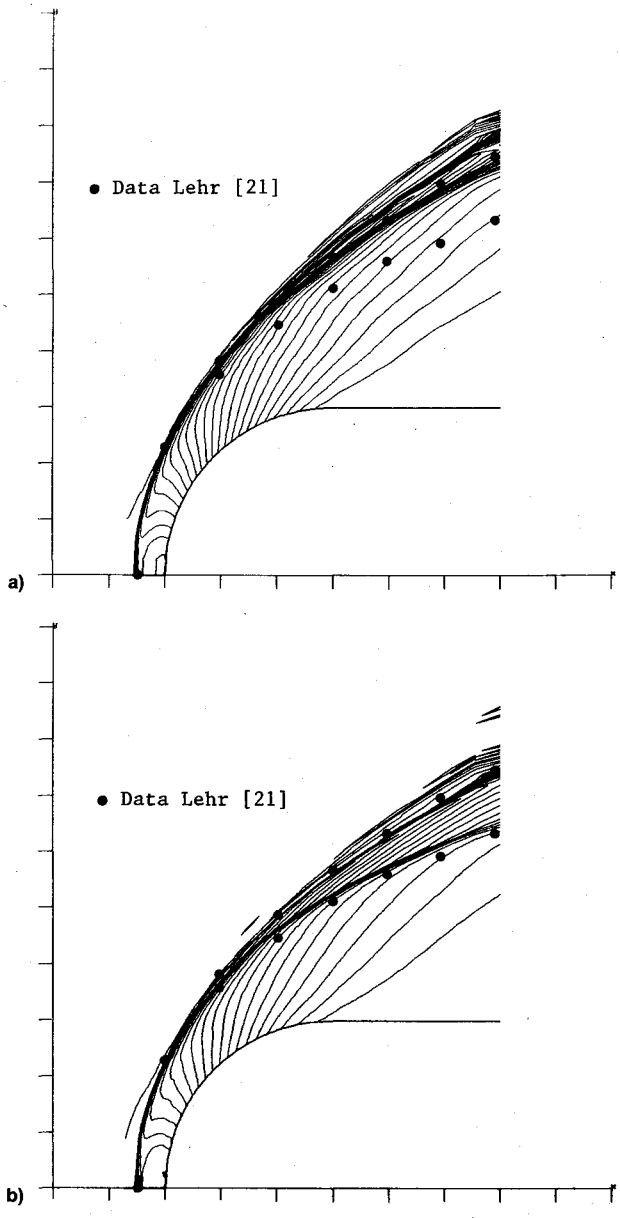


**Fig. 7 TRI3D simulation of blunt-body shock-induced combustion: a) same grid resolution as CRAFT, 5041 nodes and b) refined grid resolution, 10,011 nodes.**

equately. We base this observation on the fact that in the earlier one-dimensional premixed flame calculation (Fig. 4, with the original TVD limiter) increased grid resolution did not improve the solution since the dissipation associated with the limiter was overriding the dissipation generated by the grid skewness.

### Duct Flow Problem

A supersonic duct geometry and the representative unstructured grid is shown in Fig. 8. The three-dimensional grid was obtained with taking two parallel planes of this grid and splitting the resulting prismatic elements into tetrahedrons by adding a node point at the centroid. The length of the duct is 10 cm and its height is 1 cm, with the bump having an effective angle of 8.5 deg. The Mach number at the inflow plane is 3 and the properties of the mixture are as follows: $P = 1$ atm, $T = 1000$ K, $H_2 = 0.3$ (mole fraction), $O_2 = 0.15$, and $N_2 = 0.55$. The calculations were first performed using CRAFT, and a grid-converged solution was obtained for a 401 × 51 grid (20,451 nodes). The unstructured code TRI3D was also run for a grid with the identical number of nodes (20,451), so that

**Fig. 8 Duct geometry and unstructured grid.**

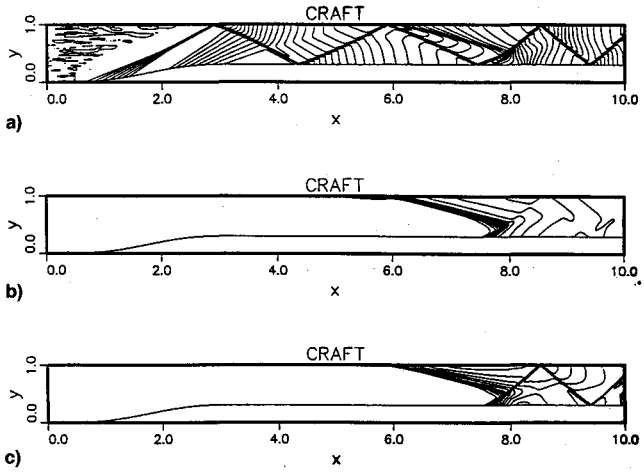


**Fig. 9 CRAFT simulation of shock-induced combustion in duct: a) density, b) water mole fractions, and c) OH mole fractions.**

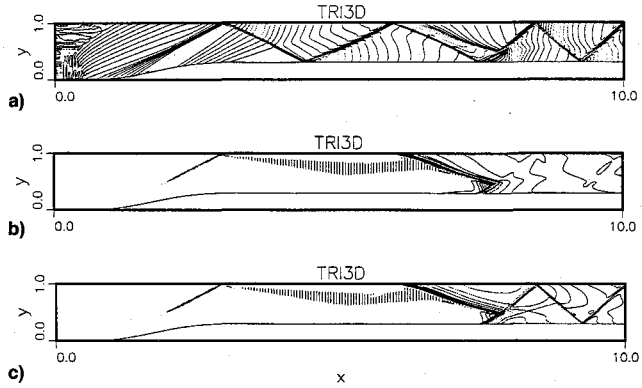


**Fig. 10 TRI3D simulation of shock-induced combustion in duct: a) density, b) water mole fractions, and c) OH mole fractions.**

comparisons could be made for similar grid resolutions. The CRAFT solution is shown in Fig. 9. The density contours in Fig. 9a indicate that combustion is initiated after the fourth shock, as it reflects from the top surface, at approximately $x = 6$ cm. The separation of the flame front from the shock is clearly evident both from the shock as well as the mass fraction contours for water and OH radical. As the temperature rises behind the flame front, the Mach number drops, and consequently, the shock angle reduces and a kink is generated in the density contours.

The corresponding results obtained using the unstructured TRI3D code are shown in Fig. 10. The results from the unstructured code generally compare well with the CRAFT solution. However, a closer inspection indicates that the flame front does not separate from the shock. This is consistent with our earlier calculation, which also indicated that the unstructured solver is generally more dissipative than the structured code for similar grid resolutions. This indicates that dynamic grid adaption is routinely required in unstructured solution procedures to capture gradients accurately. This is particularly the case for contact surfaces and flame fronts, more so than shocks, which appear to be not affected as strongly.

## Concluding Remarks

This article has focused on the methodology developed to extend the cell-vertex based unstructured TRI3D code of Barth

to accurately analyze gas-phase combusting flowfield problems. Comparative studies of complex three-dimensional aerodynamic flow problems (missile, aircraft, and rotorcraft) have been performed with TRI3D for ideal-gas cases by Barth, Strawn, and coworkers. For aerodynamic problems with strong discontinuities (e.g., hypersonic flows), the Riemann-based upwind methodology in TRI3D provides more accuracy on a point-to-point basis than codes with pressure-based solvers or solvers using central-difference numerics. However, previous studies, and this study, indicate that the accuracy of unstructured solvers, in general, is below that of structured solvers with comparable numerics because of grid alignment and flux construction issues. Significant attention has been paid to this aspect as it impacts the analysis of combusting flows with thin flame zones. The requirement for solution-adaptive gridding and improved flux limiters is clearly indicated. Comparative studies of structured and unstructured solutions of combustion flowfields, both using the same Roe/TVD flux construction, highlight differences and the need for additional care in extending unstructured solvers to this class of flows. With improved flux limiters, comparable solutions were achieved, but the grid density of unstructured solutions was always higher. Unstructured solvers with comparable numerics for combustion problems are presently unavailable for comparative studies. Studies have been limited to simple geometries and noncomplex flows in the work presented. However, the code is applicable to the analysis of complex three-dimensional flows, and work towards analyzing such problems is now in progress.

The work described represents a major step towards the development of a three-dimensional hybrid structured/unstructured solver utilizing upwind numerics. The structured solver, CRAFT, already contains advanced thermochemical capabilities for multiphase combusting flows,[11] but has limitations in analyzing flows with complex geometries, with complex dynamics, and/or with multiple-body characteristics, steady or dynamic. For complex flows, a hybrid approach that would, for example, utilize a structured solver about each body and connect the intervening domain with an unstructured solution, appears most practical and is a significant improvement over chimera-based solutions. Towards this end, S/U coupling has been formulated and tested, and preliminary particulate capabilities have been incorporated into the unstructured solver as described in Ref. 22. Work is continuing towards the development of this generalized S/U solver.

## Acknowledgments

Portions of this work were supported by a phase I Small Business Innovative Research monitored by U.S. Army Missile Command. Use of the National Academy of Sciences' Cray CPU time is acknowledged, as are technical inputs from T. Barth and R. Strawn at NASA Ames Research Center, concerning details of TRI3D code numerics.

## References

[1]Applebaum, M. P., Walters, R. W., and McGrory, W. D., "A Three-Dimensional Real-Gas Navier-Stokes Method for Unstructured Meshes," AIAA Paper 95-0095, Jan. 1995.

[2]Weiss, J. M., and Murthy, J. Y., "Computation of Reacting Flowfields Using Unstructured Adapted Meshes," AIAA Paper 95-0870, Jan. 1995.

[3]Yu, S.-T., Jiang, B.-N., Liu, N.-S., and Wu, J., "Simulation of H2/O2 Flame by the Least-Squares Finite Element Method," AIAA Paper 94-3046, June 1994.

[4]Van Leer, B., "Flux Vector Splitting for the Euler Equations," *Lecture Notes in Physics*, Vol. 170, ISBN 0-387-11948-5, Springer–Verlag, New York, 1982.

[5]Barth, T. J., "A 3-D Upwind Euler Solver for Unstructured Meshes," AIAA Paper 91-1548, June 1991.

[6]Strawn, R., Garceau, M., and Biswas, R., "Unstructured Adaptive Mesh Computations of Rotorcraft High-Speed Impulsive Noise," AIAA Paper 93-4359, Oct. 1993.

[7]Luo, H., Baum, J. D., and Löhner, R., "Edge-Based Finite Element Scheme for the Euler Equations," *AIAA Journal*, Vol. 32, No. 6, 1994, pp. 1183–1190.

[8]Cabello, J., Morgan, K., and Löhner, R., "A Comparison of Higher Order Schemes Used in a Finite Volume Solver for Unstructured Grids," AIAA Paper 94-2293, June 1994.

[9]Barth, T. J., "Numerical Aspects of Computing Viscous High Reynolds Number Flows on Unstructured Meshes," AIAA Paper 91-0721, Jan. 1991.

[10]Hosangadi, A., Sinha, N., York, B. J., and Dash, S. M., "Progress Towards the Analysis of Transient Combusting, Multiphase Flows Using Upwind/Implicit Numerics," AIAA Paper 93-0238, Jan. 1993.

[11]Sinha, N., and Dash, S. M., "Large Eddy Simulation of Jets Using Structured Upwind Numerics," Chemical Propulsion Information Agency Publication 621, Vol. 1, Oct. 1994.

[12]Barth, T. J., and Linton, S. W., "An Unstructured Mesh Newton Solution for Compressible Fluid Flow and Its Parallel Implementation," AIAA Paper 95-0221, Jan. 1995.

[13]Jacon, F., and Knight, D. D., "A Navier-Stokes Algorithm for Turbulent Flows Using An Unstructured Grid and Flux Difference Splitting," AIAA Paper 94-2292, June 1994.

[14]Evans, J. S., and Schnexnayder, C. J., Jr., "Critical Influence of Finite-Rate Chemistry and Unmixedness on Ignition and Combustion of Supersonic $H_2$/Air Streams," AIAA Paper 79-0355, Jan. 1979.

[15]Roe, P. L., "Approximate Reimann Solvers, Parameter Vectors, and Difference Schemes," *Journal of Computational Physics*, Vol. 43, 1983, pp. 357–372.

[16]Liu, K., and Vinokur, M., "Upwind Algorithms for General Thermo-Chemical Nonequilibrium Flows," AIAA Paper 89-0201, Jan. 1989.

[17]Molvik, G. A., "A Computation Model for the Prediction of Hypersonic, Reacting Flows," Ph.D. Dissertation, Dept. of Mechanical Engineering, Penn State Univ., University Park, PA, 1989.

[18]Lacor, C., and Hirsch, C., "Genuinely Upwind Algorithms for the Multidimensional Euler Equations," *AIAA Journal*, Vol. 30, No. 1, 1992, pp. 56–63.

[19]Venkatakrishnan, V., "On the Accuracy of Limiters and Convergence to Steady-State Solutions," AIAA Paper 93-0880, Jan. 1993.

[20]Pulliam, T. H., and Steger, J. L., "On Implicit Finite-Difference Simulations of Three-Dimensional Flows," AIAA Paper 78-10, Jan. 1978.

[21]Lehr, H. F., "Experiments on Shock-Induced Combustion," *Astronautica Acta*, Vol. 17, Nos. 4 and 5, 1972, pp. 589–596.

[22]Hosangadi, A., Lee, R. A., York, B. J., Sinha, N., and Dash, S. M., "A Three-Dimensional Flow Solver for Reacting Multiphase Propulsive Flows," AIAA Paper 95-0258, Jan. 1995.